Supporting Information

Tuning Methane Activation Chemistry on Alkaline Earth Metal Oxides by Doping

Hassan Aljama[1], Jens K. Nørskov[1,2], Frank Abild-Pedersen[2*]

[1]Department of Chemical Engineering, Stanford University, 443 Via Ortega, Stanford, CA 94305, United States

[2]SUNCAT Center of Interface Science and Catalysis, SLAC National Accelerator Laboratory, 2575 Sand Hill Road, Menlo Park, CA 94025, United States

*Corresponding Author e-mail: abild@slac.stanford.edu

Binding Energies

The hydrogen binding energy (E_H), the methyl binding energy (E_{CH3}), the oxygen vacancy formation energy (E_O), the C-H bond transition state energy (ΔE_{TS}), and the final state energy (ΔE_{FS}) are calculated following the same definitions as in Ref[1]:

$$E_H = E_{H*} - E_* - \frac{1}{2} E_{H_2(g)} \quad \text{(eqn. S1)}$$

$$E_{CH3} = E_{CH_3*} - E_* - E_{CH_4(g)} + 0.5\, E_{H_2(g)} \quad \text{(eqn. S2)}$$

$$E_{O-formation} = E_* - E_v - \frac{1}{2} E_{O_2(g)} \quad \text{(eqn. S3)}$$

$$\Delta E_{TS} = E_{CH_3-H*} - E_* - E_{CH_4(g)} \quad \text{(eqn. S4)}$$

$$\Delta E_{FS} = E_{CH_3*+H*} - E_* - E_{CH_4(g)} \quad \text{(eqn. S5)}$$

where E_{H*} is the total energy of H* adsorbed on the clean surface (on the oxygen next to the dopant metal atom), E_* is the total energy of the clean surface, $E_{H_2(g)}$ is the hydrogen gas phase energy, E_{CH3*} is the total energy of CH_3 adsorbed on the clean surface (on the dopant metal atom), $E_{CH_4(g)}$ is the gas phase energy of methane, E_v is the total energy of the clean surface with an oxygen vacancy (next to the dopant metal atom), $E_{O_2(g)}$ is the oxygen gas phase energy, E_{CH_3-H*} is the total energy of the transition state, and E_{CH_3*+H*} is the total energy of the true final state where CH_3 and H are on the same unit cell. Adsorption energies for surfaces studied in this work are in Table S1.

Table S1. Adsorption energy of hydrogen (E_H), methyl (E_{CH3}), and oxygen vacancy (E_O) on doped-AEMO

	E_H (eV)	E_O (eV)	E_{CH3} (eV)
Ca-MgO	0.44	-5.28	2.36
Mg-CaO	-0.83	-4.46	1.78
Sr-CaO	-0.33	-4.57	2.24
Mg-SrO	-1.03	-3.81	1.83
Ca-SrO	-1.00	-3.78	1.95
Au-MgO	-1.61	-2.45	1.21
Ag-MgO	-1.55	-2.80	1.99
Pt-MgO	-1.05	-2.33	-0.55
Pd-MgO	-1.23	-2.57	0.23
Cu-MgO	-1.59	-3.21	1.67
Ni-MgO	-0.88	-3.96	0.48
Fe-MgO	-0.14	-4.66	0.96
Co-MgO	-0.65	-4.33	0.61
Rh-MgO	-0.81	-3.74	-0.21
Ag-CaO	-2.09	-2.21	1.43
Pd-CaO	-1.73	-2.08	0.22
Rh-CaO	-1.31	-3.20	0.15

Phase diagram

Ab-initio thermodynamics was used to study the effects of water on the relative stability of AEMO(110) surface with different hydroxyl coverages. The thermodynamically favorable surface is the one with the lowest Gibbs free energy:

$$\Delta G = G^{slab}_{H*/AEMO} - G^{clean}_{AEMO} - \frac{1}{2} N_H G_{H_2O} + \frac{1}{4} N_H G_O \quad (eqn. S6)$$

For which ΔG is relative to the clean surface. $G^{slab}_{H*/AEMO}$ is the Gibbs free energy of the surface with adsorbed hydrogen, G^{clean}_{AEMO} is the Gibbs free energy of the clean surface, $G_{H_2O}$is the Gibbs free energy of the water molecule (which is equivalent to the chemical potential of water), $G_O$is the Gibbs free energy of the oxygen molecule, and $N_H$is the total number of adsorbed hydrogens. Figure S1 shows the impact of water chemical potential on MgO(110), CaO(110), and SrO(110) surface sites. SrO(110) can form a hydroxide phase at an earlier water chemical potential compared to MgO(110) and CaO(110).

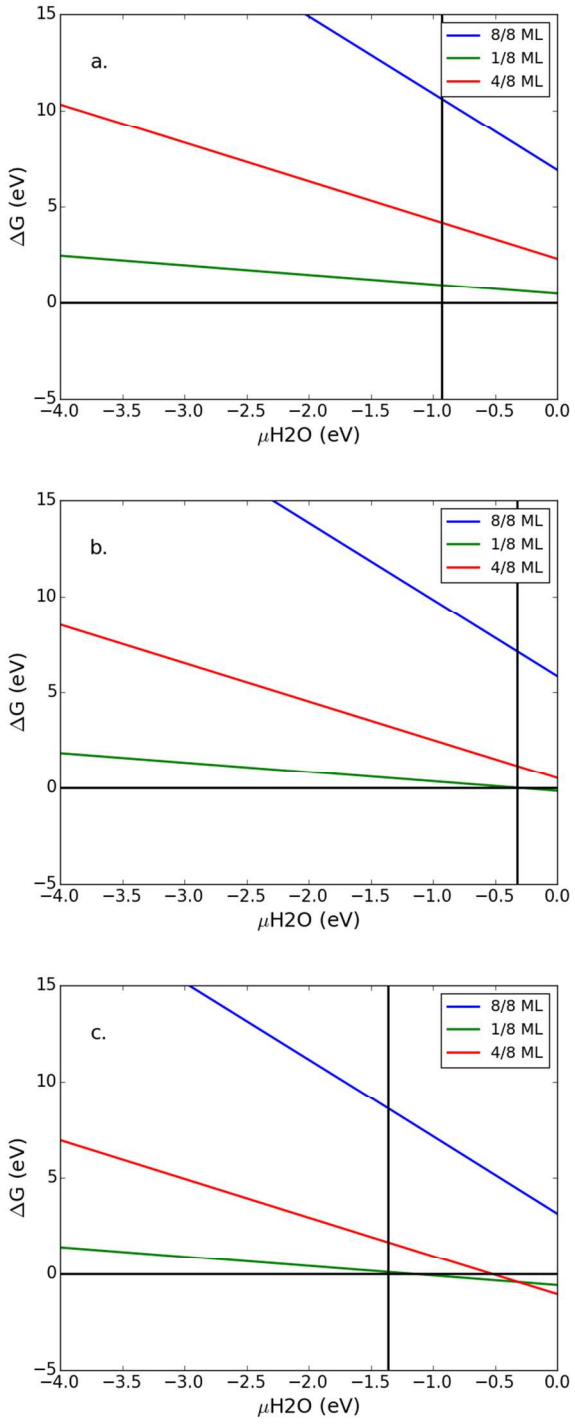

Figure S1: Phase diagram of a. MgO(110), b. CaO(110) and c. SrO(110) as a function of H_2O chemical potential at different hydroxyl coverages. The horizontal line refers to the reference energy of the pure oxide. The solid black vertical line refers to the heat of formation of the hydroxide phase. The legends to refer to the hydroxyl coverage.

Transition State Calculations

Figures S2 and S3 show the possible pathways for C-H bond dissociation on AEM-doped AEMO and TM-doped AEMO, respectively. In the case of AEM-doped AEMO, there are three distinct pathways. In the case of TM-doped AEMO, there are 5 distinct pathways.

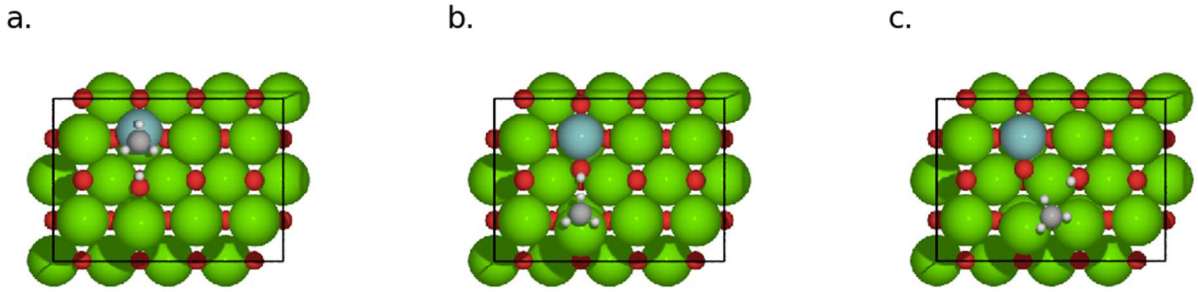

Figure S2. Surface mediated methane C-H bond activation pathway possibilities on AEM-doped AEMO. There is also the possibility of an equivalent radical-like pathway where CH_3 does not bind to the surface (Green=Mg, blue=Ca, and red=O)

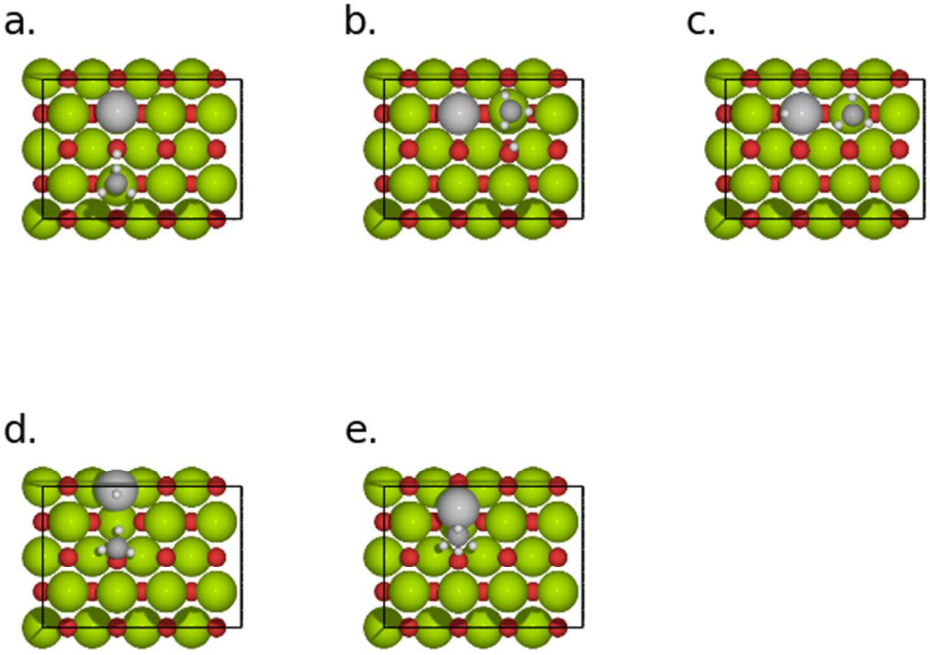

Figure S3. Surface mediated methane C-H bond activation pathway possibilities on TM-doped AEMO. There is also the possibility of an equivalent radical-like pathway where CH_3 does not bind to the surface (Green=Mg, grey=Ag and red=O)

Impact of Dopant Concentration

Figure S4 shows four different structures of CaO doped with two Magnesium atoms at different surface positions. The relative energy of surfaces shown in Figures S4b, S4c, S4d relative to Figure S4a are shown in Table S2. The structure in Figure S4c is the most stable, as shown by the lowest relative surface energy, and it is where the Magnesium dopant atoms are furthest apart.

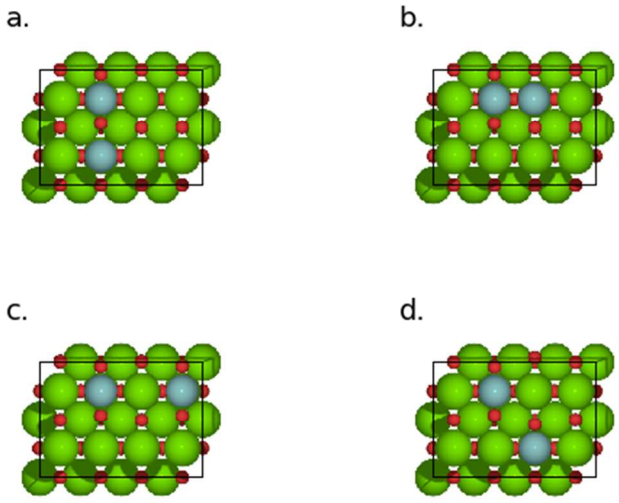

Figure S4. CaO unit cell doped with 2 Magnesium atoms at different surface locations. The surface energy of c. is more favorable, which is also where the dopant Mg atoms are furthest apart. (Green=Ca, blue=Mg and red=O)

Table S2. Relative energy of surfaces shown in Figure S4 to the energy of Surface S4a

	Relative energy to surface in Figure 4a
Figure S4a	0
Figure S4b	-0.17
Figure S4c	-0.47
Figure S4d	-0.30

Transition State Energy Calculations

Tables S3 and S4 show transition state predictions based on scaling lines in Ref[1,2]. For AEM-doped AEMO, there are 3 transition state energy predictions, each corresponding to one of the 3 structures in Figure S2. For TM-doped AEMO, there are 5 different transition state predictions, each corresponding to one of the 5 structures presented in Figure S3. We also compare the scaling line predictions to the more accurate Climbing-image nudge elastic band (CI-neb) calculation (Table S5). Results indicate the scaling lines under-predicts the transition state energy by around 0.2 eV in most cases.

Table S3. Transition state energy prediction for AEM-doped AEMO for structures shown in Figure S2 based on transition state scaling lines in Ref[1,2]

	Figure S2.a	Figure S2.b	Figure S2.c
Ca-MgO	1.20	1.04	0.62
Mg-CaO	0.07	0.23	0.17
Sr-CaO	0.92	0.78	0.66
Mg-SrO	0.08	0.33	0.59
Ca-SrO	0.39	0.42	0.60

Table S4. Transition state energy prediction for TM-doped MgO for structures shown in Figure S3 based on transition state scaling lines in Ref[1,2]

	Figure S3.a	Figure S3.b	Figure S3.c	Figure S3.d	Figure S3.e
Au	0.89	0.76	2.04	0	0
Ag	0.92	0.74	2.63	0.66	0
Pt	0.78	0	0	0	0
Pd	0.73	0	0.53	0.36	0
Cu	0.48	0.71	2.24	0.91	0
Ni	0.47	0.63	0.92	0.62	0.92
Fe	0.66	0.69	1.56	1.12	0.45
Co	0.20	0.67	1.14	0.89	0.21
Rh	0.72	0	0.03	0.35	0

Table S5. Comparison of transition state energy between full CI-neb calculations and scaling lines from Ref[1,2] based on different sites corresponding to Figures S2 and S3

		CI-neb	Scaling Line Prediction	Absolute Error
Au-MgO	Figure S3.a-radical pathway	1.00	0.80	0.20
Ag-MgO	Figure S3.a-radical pathway	1.02	0.83	0.19
Ag-MgO	Figure S3.b-radical pathway	1.02	0.78	0.24
Mg-CaO	Figure S2.a	0.17	0.07	0.10
Mg-CaO	Figure S2.b	0.00	0.23	0.22
Mg-CaO	Figure S3.e	0.26	0.17	0.09
Pt-MgO	Figure S3.e	-0.03	0	0.03

Stability of Doped Surface:

We studied the relative stability of a number of TM-doped surfaces as a function of the position of the dopant atom. Table S6 compares the relative energy when the dopant atom is in the sub-surface (the second oxide layer) to the dopant atom being in the first oxide layer (in both cases, the dopant atom is substituting an AEM atom. The positive energy of all these surfaces indicate the TM dopant atom is more stable in on-the surface position compared to the sub-surface position.

Table S6. Relative energy of sub-surface TM-doped surfaces (where dopant atom is substituting an AEM atom in the second layer) to on-surface doped surfaces (where the dopant atom is substituting a surface metal atom). In all of the presented cases the sub-surface is less stable by >1 eV.

	Sub-surface (eV)
Au-doped MgO	+3.29
Ag-doped MgO	+2.59
Pt-doped MgO	+2.12
Pd-doped MgO	+1.78
Cu-doped MgO	+1.06

Impact of Hubbard Correction:

For the 3d TM, we examined the impact of the Hubbard correction on the hydrogen binding energy (since the hydrogen binding energy is the most significant predictor of OCM on AEMO) (Table S7). Results indicate similar predictions of the BEEF-vdW exchange correlation functional to PBE+U (error is <0.2 eV).

Table S7. Impact of having Hubbard correction (+U=4) on the hydrogen binding energy of 3d TM-doped AEMO

	BEEF-vdW	**PBE+U with U=4**
Fe-MgO	-0.14	-0.29
Co-MgO	-0.66	-0.80
Ni-MgO	-0.86	-1.06

Table S7. Cartesian coordinates of MgO(110), CaO(110), and SrO(110) unit cells

MgO				CaO				SrO			
Atom#	x	y	z	Atom#	x	y	z	Atom#	x	y	z
1	0.00	0.00	8.00	1	0.00	0.00	16.00	1	0.00	0.00	16.00
2	4.50	2.12	9.50	2	5.15	2.43	17.72	2	5.54	2.61	17.85
3	1.50	2.12	9.50	3	1.72	2.43	17.72	3	1.85	2.61	17.85
4	3.00	0.00	8.00	4	3.43	0.00	16.00	4	3.69	0.00	16.00
5	3.00	2.12	8.00	5	3.43	2.43	16.00	5	3.69	2.61	16.00
6	1.50	0.00	9.50	6	1.72	0.00	17.72	6	1.85	0.00	17.85
7	4.50	0.00	9.50	7	5.15	0.00	17.72	7	5.54	0.00	17.85
8	0.00	2.12	8.00	8	0.00	2.43	16.00	8	0.00	2.61	16.00
9	3.00	4.24	11.05	9	3.43	4.85	19.48	9	3.69	5.22	19.75
10	1.50	2.12	12.52	10	1.72	2.43	21.15	10	1.85	2.61	21.55
11	4.50	2.12	12.52	11	5.15	2.43	21.15	11	5.54	2.61	21.55
12	0.00	4.24	11.05	12	6.87	4.85	19.48	12	7.39	5.22	19.75
13	0.00	2.12	11.05	13	6.87	2.43	19.51	13	7.39	2.61	19.79
14	4.50	4.24	12.54	14	5.15	4.85	21.12	14	5.54	5.22	21.49
15	1.50	4.24	12.54	15	1.72	4.85	21.12	15	1.85	5.22	21.49
16	3.00	2.12	11.05	16	3.43	2.43	19.51	16	3.69	2.61	19.79
17	0.00	4.24	14.14	17	6.87	4.85	22.96	17	7.39	5.22	23.49
18	4.50	2.12	15.46	18	5.15	2.43	24.50	18	5.54	2.60	25.18
19	1.50	2.12	15.46	19	1.72	2.43	24.50	19	1.85	2.60	25.18
20	3.00	4.24	14.14	20	3.43	4.85	22.96	20	3.69	5.22	23.49
21	3.00	2.12	14.09	21	3.43	2.43	22.99	21	3.69	2.60	23.56
22	1.50	4.24	15.53	22	1.72	4.85	24.45	22	1.85	5.22	25.06
23	4.50	4.24	15.53	23	5.15	4.85	24.45	23	5.54	5.22	25.06
24	0.00	2.12	14.09	24	0.00	2.43	22.99	24	0.00	2.60	23.56
25	0.00	4.24	8.00	25	0.00	4.85	16.00	25	0.00	5.22	16.00
26	4.50	6.36	9.50	26	5.15	7.28	17.72	26	5.54	7.84	17.85
27	1.50	6.36	9.50	27	1.72	7.28	17.72	27	1.85	7.84	17.85
28	3.00	4.24	8.00	28	3.43	4.85	16.00	28	3.69	5.22	16.00
29	3.00	6.36	8.00	29	3.43	7.28	16.00	29	3.69	7.84	16.00
30	1.50	4.24	9.50	30	1.72	4.85	17.72	30	1.85	5.22	17.85
31	4.50	4.24	9.50	31	5.15	4.85	17.72	31	5.54	5.22	17.85
32	0.00	6.36	8.00	32	0.00	7.28	16.00	32	0.00	7.84	16.00
33	3.00	8.49	11.05	33	3.43	9.71	19.48	33	3.69	10.45	19.76
34	1.50	6.36	12.52	34	1.72	7.28	21.15	34	1.85	7.84	21.55
35	4.50	6.36	12.52	35	5.15	7.28	21.15	35	5.54	7.84	21.55
36	0.00	8.49	11.05	36	6.87	9.71	19.48	36	7.39	10.45	19.76
37	0.00	6.36	11.05	37	6.87	7.28	19.51	37	7.39	7.84	19.79
38	4.50	8.49	12.54	38	5.15	9.71	21.12	38	5.54	10.45	21.49
39	1.50	8.49	12.54	39	1.72	9.71	21.12	39	1.85	10.45	21.49
40	3.00	6.36	11.05	40	3.43	7.28	19.51	40	3.69	7.84	19.79
41	0.00	8.49	14.14	41	6.87	9.71	22.96	41	7.39	10.45	23.49
42	4.50	6.36	15.46	42	5.15	7.28	24.50	42	5.54	7.85	25.18
43	1.50	6.36	15.46	43	1.72	7.28	24.50	43	1.85	7.85	25.18
44	3.00	8.49	14.14	44	3.43	9.71	22.96	44	3.69	10.45	23.49
45	3.00	6.36	14.09	45	3.43	7.28	22.99	45	3.69	7.85	23.56

46	1.50	8.49	15.53	46	1.72	9.71	24.45	46	1.85	10.45	25.07
47	4.50	8.49	15.53	47	5.15	9.71	24.45	47	5.54	10.45	25.07
48	0.00	6.36	14.09	48	0.00	7.28	22.99	48	0.00	7.85	23.56
49	6.00	0.00	8.00	49	6.87	0.00	16.00	49	7.39	0.00	16.00
50	10.50	2.12	9.50	50	12.02	2.43	17.72	50	12.93	2.61	17.85
51	7.50	2.12	9.50	51	8.58	2.43	17.72	51	9.23	2.61	17.85
52	9.00	0.00	8.00	52	10.30	0.00	16.00	52	11.08	0.00	16.00
53	9.00	2.12	8.00	53	10.30	2.43	16.00	53	11.08	2.61	16.00
54	7.50	0.00	9.50	54	8.58	0.00	17.72	54	9.23	0.00	17.85
55	10.50	0.00	9.50	55	12.02	0.00	17.72	55	12.93	0.00	17.85
56	6.00	2.12	8.00	56	6.87	2.43	16.00	56	7.39	2.61	16.00
57	9.00	4.24	11.05	57	10.30	4.85	19.48	57	11.08	5.22	19.75
58	7.50	2.12	12.52	58	8.58	2.43	21.15	58	9.23	2.61	21.55
59	10.50	2.12	12.52	59	12.02	2.43	21.15	59	12.93	2.61	21.55
60	6.00	4.24	11.05	60	13.73	4.85	19.48	60	14.78	5.22	19.75
61	6.00	2.12	11.05	61	13.73	2.43	19.51	61	14.78	2.61	19.79
62	10.50	4.24	12.54	62	12.02	4.85	21.12	62	12.93	5.22	21.49
63	7.50	4.24	12.54	63	8.58	4.85	21.12	63	9.23	5.22	21.49
64	9.00	2.12	11.05	64	10.30	2.43	19.51	64	11.08	2.61	19.79
65	6.00	4.24	14.14	65	13.73	4.85	22.96	65	14.78	5.22	23.49
66	10.50	2.12	15.46	66	12.02	2.43	24.50	66	12.93	2.60	25.18
67	7.50	2.12	15.46	67	8.58	2.43	24.50	67	9.23	2.60	25.18
68	9.00	4.24	14.14	68	10.30	4.85	22.96	68	11.08	5.22	23.49
69	9.00	2.12	14.09	69	10.30	2.43	22.99	69	11.08	2.60	23.56
70	7.50	4.24	15.53	70	8.58	4.85	24.45	70	9.23	5.22	25.06
71	10.50	4.24	15.53	71	12.02	4.85	24.45	71	12.93	5.22	25.06
72	6.00	2.12	14.09	72	6.87	2.43	22.99	72	7.39	2.60	23.56
73	6.00	4.24	8.00	73	6.87	4.85	16.00	73	7.39	5.22	16.00
74	10.50	6.36	9.50	74	12.02	7.28	17.72	74	12.93	7.84	17.85
75	7.50	6.36	9.50	75	8.58	7.28	17.72	75	9.23	7.84	17.85
76	9.00	4.24	8.00	76	10.30	4.85	16.00	76	11.08	5.22	16.00
77	9.00	6.36	8.00	77	10.30	7.28	16.00	77	11.08	7.84	16.00
78	7.50	4.24	9.50	78	8.58	4.85	17.72	78	9.23	5.22	17.85
79	10.50	4.24	9.50	79	12.02	4.85	17.72	79	12.93	5.22	17.85
80	6.00	6.36	8.00	80	6.87	7.28	16.00	80	7.39	7.84	16.00
81	9.00	8.49	11.05	81	10.30	9.71	19.48	81	11.08	10.45	19.76
82	7.50	6.36	12.52	82	8.58	7.28	21.15	82	9.23	7.84	21.55
83	10.50	6.36	12.52	83	12.02	7.28	21.15	83	12.93	7.84	21.55
84	6.00	8.49	11.05	84	13.73	9.71	19.48	84	14.78	10.45	19.76
85	6.00	6.36	11.05	85	13.73	7.28	19.51	85	14.78	7.84	19.79
86	10.50	8.49	12.54	86	12.02	9.71	21.12	86	12.93	10.45	21.49
87	7.50	8.49	12.54	87	8.58	9.71	21.12	87	9.23	10.45	21.49
88	9.00	6.36	11.05	88	10.30	7.28	19.51	88	11.08	7.84	19.79
89	6.00	8.49	14.14	89	13.73	9.71	22.96	89	14.78	10.45	23.49
90	10.50	6.36	15.46	90	12.02	7.28	24.50	90	12.93	7.85	25.18
91	7.50	6.36	15.46	91	8.58	7.28	24.50	91	9.23	7.85	25.18
92	9.00	8.49	14.14	92	10.30	9.71	22.96	92	11.08	10.45	23.49
93	9.00	6.36	14.09	93	10.30	7.28	22.99	93	11.08	7.85	23.56
94	7.50	8.49	15.53	94	8.58	9.71	24.45	94	9.23	10.45	25.07
95	10.50	8.49	15.53	95	12.02	9.71	24.45	95	12.93	10.45	25.07

96	6.00	6.36	14.09	96	6.87	7.28	22.99	96	7.39	7.85	23.56

References

(1) Aljama, H.; Nørskov, J. K.; Abild-Pedersen, F. Theoretical Insights into Methane C-H Bond Activation on Alkaline Metal Oxides. *J. Phys. Chem. C* **2017**, *121* (30), 16440–16446.

(2) Latimer, A.; Aljama, H.; Kakekhani, A.; Yoo, J. S.; Kulkarni, A.; Tsai, C.; Garcia-Melchor, M.; Abild-Pedersen, F.; Nørskov, J. K. Mechanistic Insights into Heterogeneous Methane Activation. *Phys. Chem. Chem. Phys.* **2017**, 3575–3581.